

1 **Multiphase Reaction of SO₂ on CaCO₃ Particles. 1. Oxidation of SO₂** 2 **by NO₂**

3 Defeng Zhao^{*}, Xiaojuan Song^{*}, Tong Zhu, Zefeng Zhang, Yingjun Liu

4 BIC-ESAT and SKL-ESPC, College of Environmental Sciences and Engineering, Peking University, Beijing, 100871, China

5 ^{*}These authors contributed equally to this work.

6 Correspondence to: Tong Zhu (tzhu@pku.edu.cn)

7 **Abstract.** Heterogeneous/multiphase reaction of SO₂ with NO₂ on solid or aqueous particles is thought to be a
8 potentially important source of sulfate in the atmosphere, for example, during heavily polluted episodes (haze),
9 but the reaction mechanism and rate are uncertain. In this study, we investigated the heterogeneous/multiphase
10 reaction of SO₂ with NO₂ on individual CaCO₃ particles in N₂ using Micro-Raman spectroscopy in order to
11 assess the importance of the direct oxidation of SO₂ by NO₂. In the SO₂/NO₂/H₂O/N₂ gas mixture, the CaCO₃
12 solid particle was first converted to the Ca(NO₃)₂ droplet by the reaction with NO₂ and the deliquescence of
13 Ca(NO₃)₂, and then NO₂ oxidized SO₂ in the Ca(NO₃)₂ droplet forming CaSO₄, which appeared as needle-shaped
14 crystals. Sulfate was mainly formed after the complete conversion of CaCO₃ to Ca(NO₃)₂, that is, during the
15 multiphase oxidation of SO₂ by NO₂. The precipitation of CaSO₄ from the droplet solution promoted sulfate
16 formation. The reactive uptake coefficient of SO₂ for sulfate formation is on the order of 10⁻⁸, and RH enhanced
17 the uptake coefficient. We estimate that the direct multiphase oxidation of SO₂ by NO₂ is not an important source
18 of sulfate in the ambient atmosphere compared with the SO₂ oxidation by OH in the gas phase.

20 Sulfate is a major component of atmospheric particulate matter. It contributes to a large fraction of
21 atmospheric aerosol particles in both urban and rural areas (Seinfeld and Pandis, 2006; Zhang et al., 2007).
22 Sulfate is either from primary source, such as sea spray, or from secondary source, i.e., by the oxidation of
23 reduced sulfur compounds such as dimethyl sulfide (DMS), carbonyl sulfur (COS), and SO₂ (Seinfeld and Pandis,
24 2006). In the continent, the main source of sulfate is the oxidation of SO₂, an important air pollutant from fossil
25 fuel combustion. SO₂ can be oxidized in the gas phase, mainly by OH, or in the particle phase such as by H₂O₂,
26 O₃, or O₂ catalyzed by transition metal ions in cloud or fog water (Seinfeld and Pandis, 2006; Finlayson-Pitts and
27 Pitts Jr., 1999) or by O₃ or photochemical reactions on particle surface (Zhu et al., 2011; Li et al., 2006; Li et al.,
28 2007; Shang et al., 2010; Li et al., 2011).

29 Although various pathways of SO₂ oxidation are identified, the source of sulfate and relative importance of
30 various pathways of SO₂ oxidation forming sulfate in the atmosphere still remain uncertain. For example, during
31 heavily polluted episodes (haze) in China in recent years, high concentrations of sulfate were observed, but the
32 source of sulfate is elusive (Wang et al., 2016; Wang et al., 2014a; Zheng et al., 2015b; Guo et al., 2014). The
33 relative contribution of regional transport versus local formation and physical and chemical mechanisms
34 responsible for sulfate formation are still not clear. Recent studies have highlighted heterogeneous reactions of
35 SO₂ on solid or liquid particles to be a possibly important source of sulfate based on model, field and laboratory
36 studies (Huang et al., 2014; Zhu et al., 2011; Cheng et al., 2016a; Gao et al., 2016; Zheng et al., 2015a; Wang et
37 al., 2014b; He et al., 2014; Fu et al., 2016; Xue et al., 2016; Xie et al., 2015). During haze episodes, relative
38 humidity (RH) is often high (Zhang et al., 2014; Wang et al., 2016; Zheng et al., 2015b) and particles or some
39 components of particles can deliquesce forming liquid water. In particular, several recent studies propose that the
40 multiphase oxidation of SO₂ by NO₂, another important air pollutant, on liquid particles may be a major pathway
41 of sulfate formation (Cheng et al., 2016a; Wang et al., 2016; Xue et al., 2016; Xie et al., 2015). Both SO₂ and
42 NO₂ are from fossil fuel combustion and both concentrations are often high during haze episodes, and their
43 reaction may significantly contribute to sulfate formation.

44 In order to assess and quantify the role of the heterogeneous reactions of SO₂ in sulfate formation, laboratory
45 studies are needed to understand the reaction process and obtain kinetic parameters for modeling such as uptake
46 coefficients of SO₂. Among many studies investigating the heterogeneous reactions of SO₂ on various particles
47 (Goodman et al., 2001; Li et al., 2011; Shang et al., 2010; Huang et al., 2015; Huang et al., 2016; Zhou et al.,
48 2014; Li et al., 2004; Kong et al., 2014; Passananti et al., 2016; Cui et al., 2008; Chu et al., 2016; Zhao et al.,
49 2015; Li et al., 2006; Wu et al., 2011; He et al., 2014; Liu et al., 2012; Ma et al., 2008; Park and Jang, 2016;
50 Ullerstam et al., 2002; Sorimachi et al., 2001; Ullerstam et al., 2003; Wu et al., 2013; Wu et al., 2015), only a few
51 have investigated the heterogeneous reaction of SO₂ in the presence of NO₂ (He et al., 2014; Liu et al., 2012; Ma
52 et al., 2008; Park and Jang, 2016; Ullerstam et al., 2003; Ma et al., 2017). These studies found that NO₂ can
53 promote sulfate formation from SO₂ oxidation (He et al., 2014; Liu et al., 2012; Ma et al., 2008; Park and Jang,
54 2016; Ullerstam et al., 2003). However, the mechanism of this effect is still not clear and only few studies
55 reported kinetic parameters such as uptake coefficient of SO₂ in the presence of NO₂. Importantly, most of these
56 studies focused on the gas-solid reactions on particles. Very few laboratory studies have investigated the
57 multiphase reaction of SO₂ with NO₂ on atmospheric aqueous particles or solid-aqueous mixed phase aerosol

58 particles, and the uptake coefficient of SO₂ on atmospheric aqueous particles due to the reaction with NO₂ is
59 largely unknown. From several decades ago until now, a number of studies have investigated the aqueous
60 reaction of soluble S(IV) species (H₂SO₃, HSO₃⁻, SO₃²⁻) with NO₂ in dilute bulk solution (Lee and Schwartz,
61 1983; Clifton et al., 1988; Littlejohn et al., 1993; Takeuchi et al., 1977; Nash, 1979; Ellison and Eckert, 1984;
62 Shen and Rochelle, 1998; Tursic and Grgic, 2001) relevant to the conditions in cloud water. However, in aqueous
63 aerosol particles, the reaction rate and process may be substantially different from in bulk solution due to high ion
64 strength resulted from high concentrations of solutes, potential interactions of sulfate with other ions, and low
65 water activity in aerosol particles.

66 In this study, we investigated the heterogeneous reaction of SO₂ with NO₂ on CaCO₃ particles at the ambient
67 RH. CaCO₃ is an important component of mineral aerosols, especially in East Asia (Cao et al., 2005; Song et al.,
68 2005; Okada et al., 2005) and it is a very reactive component (Krueger et al., 2004; Li et al., 2010; Li et al., 2006;
69 Prince et al., 2007a). It is also one of the few alkaline particles in the atmosphere, especially in northern China,
70 which can neutralize acids on particles and increase the pH of aerosol water, thus promoting the apparent
71 solubility and uptake of SO₂. The reaction of SO₂ with NO₂ on CaCO₃ has been suggested by field observations,
72 which showed internal mixing of CaCO₃, CaSO₄, and Ca(NO₃)₂ in particles (Hwang and Ro, 2006; Li and Shao,
73 2009; Zhang et al., 2000). More importantly, as shown below, during the reaction on CaCO₃, aqueous phase can
74 be formed, which allows us to investigate the multiphase reaction of SO₂ with NO₂. We studied the reaction of
75 SO₂ and NO₂ on individual CaCO₃ particles in N₂ using Micro-Raman spectrometer with a flow reaction system.
76 Combining the chemical and optical information from Micro-Raman spectrometer, we systematically
77 investigated the reaction process and quantified the reactive uptake coefficient of SO₂ due to the oxidation by
78 NO₂ based on sulfate production rate. We further assessed the importance of the multiphase reaction of SO₂ with
79 NO₂ in the atmosphere. In this study, we present the findings of the multiphase reaction of SO₂ directly with NO₂,
80 a reaction pathway proposed in a number of recent studies to be potentially important for sulfate formation
81 (Cheng et al., 2016b; Wang et al., 2016; Xue et al., 2016). In a companion paper, we shall report another study of
82 the multiphase reaction of SO₂ with O₂ initiated by NO₂.

83 **2 Experimental**

84 **2.1 Apparatus and procedures**

85 The experimental setup used in this study is illustrated in Fig. 1. The details of the setup have been described
86 previously (Liu et al., 2008; Zhao et al., 2011). NO₂ and SO₂ of certain concentrations were prepared by adjusting
87 the flow rates of standard gases of specified concentrations (NO₂: 1000 ppm in N₂, Messer, Germany; SO₂: 2000
88 ppm in N₂, National Institute of Metrology P.R.China) and high-purity nitrogen (99.999%, Beijing
89 Haikeyuanchang Corp.). We used N₂ as a carrier gas to exclude the potential inference from other compounds in
90 SO₂ oxidation such as O₂, which is key to investigate the direct oxidation of SO₂ by NO₂. RH was regulated by
91 adjusting the flow rates of humidified N₂ and of dry N₂ and other dry gases. Humidified N₂ was prepared by
92 bubbling N₂ through fritted glass in water. Flow rates of the gases were controlled by mass flow controllers
93 (FC-260, Tylan, Germany). Mixed gases reacted with CaCO₃ particles in a stainless steel reaction cell. Individual
94 CaCO₃ particles were deposited on a Teflon FEP film substrate annealed to a silicon wafer. The substrate was

95 then placed in the reaction cell, which has a glass cover on top of the center. Through this top window, a
96 Micro-Raman spectrometer (LabRam HR800, HORIBA Jobin Yvon) was used to acquire the Raman spectra of
97 particles. A 514 nm excitation laser was focused onto selected particles and back scattering Raman signals were
98 detected. The details of the instrument are described in previous studies (Liu et al., 2008; Zhao et al., 2011).

99 The RH and temperature of the outflow gas from the reaction cell were measured by a hygrometer (HMT100,
100 Vaisala). Experiments of individual CaCO₃ particles reacting with NO₂ (75-200 ppm) and SO₂ (75-200 ppm)
101 mixing gas diluted with N₂ were conducted under certain RH (17-72%). All the measurements were carried out at
102 25±0.5 °C. Each reaction was repeated for three times.

103 In this study, the size of CaCO₃ particles was around 7-10 μm. During a reaction, components of an
104 individual particle may distribute unevenly within the particle due to the formation of new aqueous phase or solid
105 phase, and particles may grow. Because particles are larger than the laser spot (~1.5 μm), Raman spectrum from
106 one point does not represent the chemical composition of the whole particle. Therefore Raman mapping was used
107 to obtain the spectra on different points of a particle in order to get the chemical information of the whole particle.
108 The mapping area is a rectangular slightly larger than the particle and mapping steps are 1×1 μm. Raman spectra
109 in the range 800-3900 cm⁻¹ were acquired with exposure time of 1 s for each mapping point. During each
110 mapping (7-10 min, depending on the mapping area), no noticeable change in composition was detected. The
111 mean time of a mapping period was used as reaction time. During the reaction, microscopic images of particles
112 were also recorded. Raman spectra were analyzed using Labspec 5 software (HORIBA Jobin Yvon). Raman
113 peaks were fit to Gaussian-Lorentzian functions to obtain peak positions and peak areas on different points of the
114 particle. The peak areas were then added up to get the peak area for the whole particle.

115 Besides the reaction of CaCO₃ with SO₂ and NO₂, other reaction systems including the reaction on Ca(NO₃)₂,
116 NaNO₃, NH₄NO₃ particles with SO₂ or SO₂ and NO₂ mixing gas (summarized in Table 1) were also studied in
117 order to elucidate the reaction mechanism.

118 CaCO₃ (98%, Sigma) with diameters about 7-10 μm on average, Ca(NO₃)₂·4H₂O (ACS, 99-103%; Riedel-de
119 Haën), NH₄NO₃ (AR, Beijing Chemical Works), and NaNO₃ (AR, Beijing Chemical Works) were used without
120 further purification.

121 2.2 Quantification of reaction products on the particle phase

122 The Raman intensity of a sample is described as Equation (1):

$$123 I(\nu)=I_0\cdot A(\nu)\cdot J(\nu)\cdot\nu^4\cdot D\cdot K \quad (1)$$

124 where I₀ is the intensity of incident laser, A(ν) is the collection efficiency function of Raman spectrometer,
125 J(ν)·ν⁴ is the Raman scattering section of the sample, D is the number density of the sample, and K is the
126 effective depth of the sample. Raman intensity is not only determined by the amount of the sample molecules, but
127 also by the configuration of the instrument, whose influence cannot be eliminated unless internal standards are
128 used. For soluble compounds, water can be used an internal standard (Zhao et al., 2011; Liu et al., 2008).
129 However, in this study, one product (CaSO₄, see below) appeared as solid state. For solid particles of micro-scale,
130 it is hard to add internal standards into the system. Therefore it is difficult to establish the relationship between
131 Raman intensity and the amount of sample molecules, which makes the quantification very challenging.

132 In this study, we chose seven individual CaSO₄ particles varying in size as the standard for solid products.
 133 The profile of each particle can be obtained by scanning the particle using Raman mapping with steps of 1, 1, and
 134 2 μm for x, y, and z dimension, respectively. The volume of each particle was calculated based on 3D profiles of
 135 the particles using a CAD software (AutoDesk). In order to minimize the influence variations of incident laser on
 136 Raman intensity, these seven particles were measured before each experiment, which produced a calibration
 137 curve for each experiment (Fig. S1).

138 2.3 Determination of reactive uptake coefficient

139 In this study, sulfate was produced from the oxidation of SO₂. The reactive uptake coefficient γ of SO₂ on
 140 individual particles was estimated from sulfate formation. γ is derived as the rate of sulfate formation
 141 (d{SO₄²⁻}/dt) divided by the rate of surface collisions with an individual particle (Z),

$$142 \gamma = \frac{d\{\text{SO}_4^{2-}\}}{Z} . \quad (2)$$

$$143 Z = \frac{1}{4}cA_s[\text{SO}_2], \quad (3)$$

$$144 c = \sqrt{\frac{8RT}{\pi M_{\text{SO}_2}}} , \quad (4)$$

145 where R is the gas constant, T is temperature, M_{SO₂} is the molecular weight of SO₂, and c is the mean
 146 molecular velocity of SO₂, A_s is the surface area of an individual particle. Z is the collision rate between SO₂ and
 147 a particle. {SO₄²⁻} indicates the amount of sulfate on the particle phase in mole, and [SO₂] indicates the
 148 concentration of SO₂ in the gas phase.

149 {SO₄²⁻} was determined by a calibration curve as stated above. In this study, since sulfate was mainly
 150 formed after the formation of Ca(NO₃)₂ droplet as shown below, A_s was calculated by estimating the diameter of
 151 the droplet according to its microscopic image and using a shape of spherical segment defined by the contact
 152 angle water droplet on Teflon (Good and Koo, 1979). For each experiment, at least three particles with different
 153 diameters were measured to get an average reactive uptake coefficient.

154 3 Results and discussion

155 3.1 Reaction products and particle morphology changes

156 Figure 2 shows typical Raman spectra of a CaCO₃ particle during the reaction with SO₂ and NO₂. The peak
 157 at 1087 cm⁻¹ is assigned to the symmetric stretching mode of carbonate (ν₁) (Nakamoto, 1997), which could be
 158 detected during the initial stage of the reaction. Shortly after the reaction started, a peak at 1050 cm⁻¹ was
 159 observed, which is attributed to the symmetric stretching mode of nitrate (ν₁). This demonstrates that calcium
 160 nitrate (Ca(NO₃)₂) was produced during the reaction. A broad band at 2800-3800 cm⁻¹ was also observed together
 161 with the formation of Ca(NO₃)₂. It is assigned to -OH stretching of liquid water. The formation of liquid water is
 162 attributed to the deliquescence of Ca(NO₃)₂, which is very hygroscopic and can deliquesce at ~10% RH (Liu et al.,
 163 2008; Al-Abadleh et al., 2003; Tang and Fung, 1997). After about 82 min, a new peak at 1013 cm⁻¹ was observed,
 164 which is attributed to the symmetric stretching mode of sulfate (ν₁) in anhydrite (CaSO₄) (Sarma et al., 1998).
 165 This peak clearly demonstrates that sulfate was formed. CaSO₄ as a reaction product has also been found in the

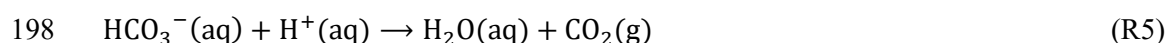
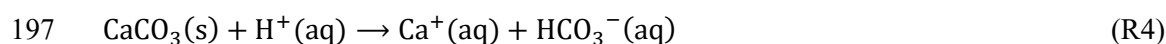
166 reaction of CaCO₃ with SO₂ and NO₂ in a previous study (Ma et al., 2013b). Afterwards, no other Raman peaks
167 than those of CaCO₃, Ca(NO₃)₂, and CaSO₄ were detected until 1050 min after the reaction.

168 Concomitant with the formation of Ca(NO₃)₂ and CaSO₄, the microscopic morphology of the particle
169 changed significantly. The initial CaCO₃ particle was a crystal close to a rhombohedron of about 9-10 μm (Fig.
170 3a). After reacting with NO₂/SO₂, the surface of the particle became smoother, and then a liquid layer formed
171 surrounding the solid particle core (Fig. 3c). Raman spectra of the particle reveal that the outer liquid layer
172 consisted of Ca(NO₃)₂ and water. As the reaction proceeded, the solid CaCO₃ core diminished gradually and
173 finally CaCO₃ completely disappeared and a Ca(NO₃)₂ spherical droplet was formed (Fig. 3d). The whole particle
174 became larger due to the growth of the outer liquid layer. The diameter of the Ca(NO₃)₂ droplet reached ~16 μm,
175 and the droplet did not change much in the subsequent period of the reaction. Despite the invariant droplet
176 diameter, a new solid phase of needle-shaped crystals was formed as the reaction proceeded, which distributed
177 unevenly in the droplet. The Raman spectra of the new solid phase and Raman mapping (Fig. S2) reveal that this
178 solid matter was CaSO₄. The amount of CaSO₄ increased gradually during the reaction, and its Raman peak could
179 be observed more clearly at 1050 min.

180 3.2 Reaction process

181 In order to learn about the reaction process and mechanism, the amounts of Ca(NO₃)₂, CaSO₄, and CaCO₃,
182 represented by the peak area at 1050, 1013, and 1087 cm⁻¹ in Raman spectra, respectively, were investigated as a
183 function of reaction time. As shown in Fig. 4, Ca(NO₃)₂ was produced before CaSO₄. Nitrate was detected
184 immediately after the reaction started, and reached a maximum at ~50 min whereas sulfate did not reach the
185 detection limit until 82 min of the reaction. Sulfate increased slowly in the reaction and we did not observe it
186 leveling off even after 1050 min.

187 According to the time series of carbonate, nitrate, and sulfate, this reaction consisted of two successive
188 processes. The first process was the formation of Ca(NO₃)₂, which was accompanied with the decline of CaCO₃
189 (Fig. 4), indicating that Ca(NO₃)₂ was produced due to the reaction of CaCO₃ with NO₂. Ca(NO₃)₂ has been
190 observed in the reaction of CaCO₃ with NO₂ in previous studies (Li et al., 2010; Tan et al., 2017). The formation
191 of Ca(NO₃)₂ started with the reaction of NO₂ with adsorbed or liquid water, forming HNO₃ and HNO₂. Then
192 HNO₃ reacted with CaCO₃ forming Ca(NO₃)₂ as well as CO₂, which was released to the gas phase. The reaction
193 equations are as follows:



199 The detailed mechanism of the formation of Ca(NO₃)₂ in the reaction CaCO₃ with NO₂ have been studied by Li et
200 al. (2010). The second process was the formation of CaSO₄ through the oxidation of SO₂. CaSO₄ was mainly
201 produced after CaCO₃ was completely reacted and increased steadily as the reaction proceeded. The much faster
202 Ca(NO₃)₂ formation due to the NO₂ uptake on CaCO₃ particle compared with the reaction of SO₂ with NO₂ and

203 sulfate appearing only after the complete conversion of CaCO₃ indicate that the reaction of SO₂ with NO₂ does
204 not contributed significantly to NO₂ uptake.

205 3.3 Reaction mechanism

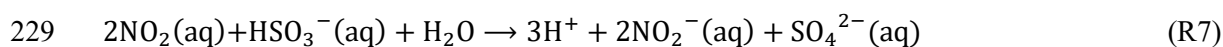
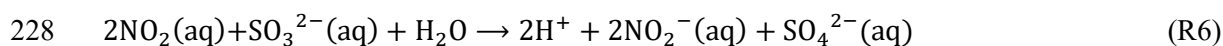
206 3.3.1 Mechanism of sulfate formation

207 Based on the results above, we found that a series of reactions of SO₂ and NO₂ on a CaCO₃ particle led to
208 sulfate formation. Almost the entire sulfate was produced after a CaCO₃ particle was converted to a Ca(NO₃)₂
209 droplet (Fig. 4), although in some experiments a trace amount of sulfate could be observed when a small amount
210 of CaCO₃ was still left in the Ca(NO₃)₂ droplet. The absence or low amount of sulfate before CaCO₃ was
211 completely reacted might be due to the competition between the reaction of aqueous NO₂ with CaCO₃ and the
212 reaction with SO₂. This result suggests that forming a Ca(NO₃)₂ droplet was key to the formation of sulfate.

213 This finding is further supported by the results of the reaction of SO₂ with NO₂ on a Ca(NO₃)₂ droplet (Fig. 5
214 and Table 1). Using a Ca(NO₃)₂ droplet as the reactant, the reaction with SO₂/NO₂ at the same condition still
215 produced CaSO₄, confirming CaCO₃ was not necessary for sulfate formation. The reaction with Ca(NO₃)₂
216 produced similar amount of sulfate to the reaction with CaCO₃ based on Raman spectra and microscopic images
217 (Fig. 5), which indicates that Ca(NO₃)₂ droplet was important for sulfate formation. Therefore, we conclude that
218 SO₂ was mainly oxidized via the multiphase reaction on the Ca(NO₃)₂ droplet while CaCO₃ mainly worked as a
219 precursor of the Ca(NO₃)₂ droplet.

220 The oxidant of SO₂ can be NO₃⁻ or NO₂ in the Ca(NO₃)₂ droplet here. In a reaction between Ca(NO₃)₂
221 droplets and SO₂ (150 ppm) under 72% RH, we did not observe any sulfate formation on the basis of the Raman
222 spectra and microscopic image after 5 h of reaction. This indicates that NO₃⁻ was not the oxidant for SO₂ in our
223 study, which was also consistent with a previous study (Martin et al., 1981). Therefore, we conclude that SO₂ was
224 oxidized by NO₂ in the Ca(NO₃)₂ droplet.

225 According to previous studies, NO₂ can oxidize sulfite and bisulfite ions into sulfate ion in aqueous phase
226 (Ellison and Eckert, 1984; Shen and Rochelle, 1998; Littlejohn et al., 1993). The overall mechanism was
227 described to be (Clifton et al., 1988):



230 Under the experimental conditions of our study, water uptake of Ca(NO₃)₂ led to condensation of liquid
231 water, which provided a site for aqueous oxidation of S(IV) by NO₂. The relative fractions of the three S(IV)
232 species depend on pH and the equilibrium between them is fast (Seinfeld and Pandis, 2006). The pH of the
233 droplet was mainly determined by the gas-aqueous equilibrium of SO₂ in this study and estimated to be ~3. The
234 concentrations of HSO₃⁻, H₂SO₃, and SO₃²⁻ were estimate to be ~1.1×10⁻³, 9.2×10⁻⁵, and 6.6×10⁻⁸ mol L⁻¹,
235 respectively, using the equilibrium constants in Seinfeld and Pandis (2006) and thus the main S(IV) species was
236 HSO₃⁻. Then SO₄²⁻ from S(IV) oxidation can react with Ca²⁺ forming CaSO₄ precipitation as observed in Raman
237 spectra due to the low value of K_{sp} for CaSO₄ (Lide, 2009):



239 Some previous studies have shown that SO₂ can react with CaCO₃ to produce calcium sulfite (CaSO₃) (Li et
 240 al., 2006; Prince et al., 2007b; Ma et al., 2013a), and CaSO₃ can be oxidized to CaSO₄ by NO₂ (Rosenberg and
 241 Grotta, 1980; Ma et al., 2013a). In our study, we investigated the reaction between CaCO₃ and SO₂ (150 ppm) at
 242 72% RH. We found that both sulfate and sulfite were lower than the detection limit of our Raman spectrometer
 243 even after 300 min of the reaction. This indicates that forming CaSO₃ was not the main pathway in CaSO₄
 244 formation in our study and CaCO₃ did not directly contribute to the formation of CaSO₄.

245 3.3.2 Effects of cations in sulfate formation

246 Since sulfate was observed to precipitate as CaSO₄, we further analyzed the effect of precipitation reaction
 247 and cations on the aqueous oxidation of SO₂ by NO₂. In order to test effects of cations, we replaced Ca²⁺ with Na⁺
 248 or NH₄⁺. Based on Raman spectra, we found that in the reaction of a NaNO₃ or a NH₄NO₃ droplet with NO₂/SO₂
 249 sulfate was below the detection limit after 300 min in the same reaction conditions as Ca(NO₃)₂ and CaCO₃ (Fig.
 250 6 and Table 1). Accordingly, no sulfate solid particles were observed in these droplets. Clearly, the sulfate
 251 production rate was larger in the presence of Ca²⁺ compared to those in the presence of Na⁺ or NH₄⁺. The
 252 difference can be explained by the change of Gibbs energy. The spontaneity of the SO₂ oxidation by NO₂ for
 253 Reaction (R2) can be analyzed using the reaction Gibbs energy as follows:

$$254 \Delta_r G = \Delta_r G^\theta + RT \ln \frac{a_{H^+}^3 \cdot a_{SO_4^{2-}} \cdot a_{NO_2^-}^2}{a_{NO_2(aq)}^2 \cdot a_{HSO_3^-}} \quad (5)$$

255 where Δ_rG is the reaction Gibbs energy, Δ_rG^θ is the standard reaction Gibbs energy, R is the gas constant, T
 256 is temperature, and a is the activity of various species.

257 Δ_rG increases with increasing sulfate concentration. According to the different results between the reaction
 258 on Ca(NO₃)₂ droplet and the reaction on NaNO₃ and NH₄NO₃ droplet, there might be a backward reaction of SO₂
 259 oxidation which consumed sulfate, although the detailed mechanism of the backward reaction is unknown at the
 260 moment. For NaNO₃ and NH₄NO₃ droplet, once sulfate concentration reached certain level, the reaction may stop
 261 due to the increase of Δ_rG. For Ca(NO₃)₂ droplet, the precipitation of CaSO₄ can substantially decrease the
 262 activity of SO₄²⁻, and thus decrease Δ_rG and promote the oxidation of SO₂ and sulfate formation. Therefore, we
 263 can conclude that the precipitation of less soluble CaSO₄ promoted sulfate formation.

264 3.4 Reactive uptake coefficient of SO₂

265 The reactive uptake coefficients of SO₂ (γ) for sulfate formation under different conditions are shown in
 266 Table 2. Each reaction was repeated for three times, during which, three particles with different size were
 267 selected. γ was higher at higher relative humidity, suggesting again that liquid water plays an important role in
 268 the formation of CaSO₄. At 17% RH, the reaction between CaCO₃ and NO₂ (the first process of the whole
 269 reaction) proceeded very slowly, and the amount of liquid water formed due to the water uptake of Ca(NO₃)₂ was
 270 very low. As a result, we did not observe the formation of CaSO₄ (the second process of the whole reaction) after
 271 1000 min of the reaction and even at higher SO₂ and NO₂ concentrations (200 ppm SO₂, 200 ppm NO₂). Under
 272 higher relative humidity (46% and 72% RH), sulfate was observed soon after the reaction. It is interesting to note
 273 that there were no significant difference for γ between 46% and 72% RH. In either case, the reaction between
 274 CaCO₃ and NO₂ proceeded quickly and CaCO₃ was completely converted to a Ca(NO₃)₂ droplet within 100 min

275 after the reaction. In the presence of enough liquid water, RH seemed to be no longer a limiting factor. In such
276 conditions, an increase of NO₂ concentration (from 75 ppm to 200 ppm at 72% RH) promoted the reactive uptake
277 of SO₂.

278 The reactive uptake coefficient of SO₂ for sulfate formation was determined to be on the order of 10⁻⁸ at 46%
279 and 72% RH. This value is higher than the uptake coefficient (10⁻¹⁰) on mineral particles sampled from Cape
280 Verde Islands (the main contents being potassium feldspars and quartz) obtained by Ullerstam et al. (2003) using
281 NO₂/SO₂ mixing gas and Diffuse Reflectance Infrared Fourier Transform Spectroscopy (DRIFTS) technique. But
282 the uptake coefficient in this study is lower than the uptake coefficient of SO₂ on Arizona Test Dust (ATD)
283 particles in the presence of NO₂ ((2.10±0.08)×10⁻⁶) determined by Park and Jang (2016). γ here is also much
284 lower than the γ of SO₂ on oxalic acid particles in the presence of NO₂ and NH₃ (10⁻⁶~10⁻⁴) determined at varying
285 RH reported by Wang et al. (2016). The difference in these uptake coefficients is attributed to the different
286 chemical composition of particles, reaction mechanism, reaction conditions, and the ways that the particle surface
287 is determined. It is worth noting that in the studies of Ullerstam et al. (2003) and Park and Jang (2016), particles
288 exist as solid state and sulfate formation is via gas-solid heterogeneous reaction, and in the study of Wang et al.
289 (2016) sulfate formation is stated to be via aqueous reaction. In this study sulfate formation was via
290 gas-liquid-solid multiphase reaction and liquid water played a key role.

291 The γ of SO₂ was further compared with the reaction rate constants of the aqueous reaction of NO₂ with
292 sulfite and bisulfite in bulk solution in the literature by deriving γ from rate constants using the method in
293 Davidovits et al. (2006). The detailed method can be referred to the supplement S1. Lee and Schwartz (1983)
294 determined the rate constant of the reaction of NO₂ with bisulfite to be >2×10⁶ mol⁻¹ L s⁻¹ at pH 5.8 and 6.4.
295 Clifton et al. (1988) determined the rate constant of the reaction of NO₂ with sulfite/bisulfite to be
296 (1.24-2.95)×10⁷ mol⁻¹ L s⁻¹ at pH 5.6-13 and further reported a rate constant of 1.4×10⁵ mol⁻¹ L s⁻¹ at pH 5 from
297 the study of Lee and Schwartz (1983). The different rate constants were attributed to the different approaches to
298 determine the reaction rate by Clifton et al. (1988). Clifton et al. (1988) determined the reaction rate from the
299 consumption rate the reactant, NO₂, which corresponds to the first reaction step of NO₂ with S(IV). Yet, Lee and
300 Schwartz (1983) determined the reaction rate from the production rate of products (their conductivity), which is
301 expected to be much slower than NO₂ consumption since formation of products needs more steps. In this study,
302 we determined γ using sulfate production rate, and thus our data are comparable to the study of Lee and Schwartz
303 (1983). Yet, the study of Lee and Schwartz (1983) only covers a pH range of 5-6.4 and has no overlap with the
304 pH (~3) in our study, therefore uptake coefficients from both studies are not directly comparable. Nevertheless,
305 the reaction rate of 1.4×10⁵ mol⁻¹ L s⁻¹ at pH 5 corresponds to the uptake coefficient of 4.3×10⁻⁷, which is around
306 one order of magnitude higher than the uptake coefficient in our study determined at pH ~3 for the droplet. The
307 difference may be due to the different pH between these two studies, the different mechanisms between the
308 multiphase reaction on particles and bulk aqueous reaction, and the different concentrations of each S(IV) species
309 since the different species may have different reactivity with NO₂. The reaction rate of S(IV) has been found to
310 decrease with decreasing pH and the reactivity of sulfite with NO₂ seems to be higher than bisulfite (Lee and
311 Schwartz, 1983; Clifton et al., 1988; Takeuchi et al., 1977). In addition, the ionic strength in the droplet of this
312 study (15-55 mol Kg⁻¹) was much higher than that in the bulk solution in previous studies (on the order of
313 10⁻⁶-10⁻¹ mol Kg⁻¹), which may also influence the reaction rate.

314 In the ambient atmosphere, the reactive uptake coefficient of SO₂ due to the multiphase oxidation by NO₂ is
315 influenced by various factors such as RH, NO₂ concentration, pH, sulfate concentration, and the presence of other
316 ions in aerosol particles. For example, NO₂ concentrations in the atmosphere are much lower than those used in
317 this study. At lower NO₂ concentrations, the uptake coefficient of SO₂ decreases, because the oxidation rate of
318 SO₂ in aqueous phase decreases with decreasing NO₂ concentration. In addition, aqueous sulfate concentrations
319 in aerosol particles in the atmosphere are often high. According to the effect of cations (Section 3.3.2), while
320 reduced sulfate concentration by CaSO₄ precipitation likely led to the enhanced sulfate production rate in the
321 reaction of SO₂ on Ca(NO₃)₂, higher sulfate concentration could increase the reaction Gibbs energy Δ_rG (as
322 shown in Eq. 5) and thus suppress the reaction of SO₂ and NO₂. This can reduce the uptake coefficient of SO₂.
323 Therefore, the reactive uptake coefficient of SO₂ obtained in this study (10⁻⁸ at 46-72% RH and 75 ppm NO₂) can
324 be regarded as an upper limit of the reactive uptake coefficient of SO₂ due to the multiphase reaction with NO₂ in
325 the ambient atmosphere.

326 4 Conclusion and implications

327 We investigated the heterogeneous reaction of SO₂ directly with NO₂ on individual CaCO₃ particles in N₂
328 using Micro-Raman spectrometry. The reaction first converted the CaCO₃ particle to the Ca(NO₃)₂ droplet via the
329 reaction with NO₂ in the SO₂/NO₂/H₂O/N₂ gas mixture and the deliquescence of Ca(NO₃)₂, and then formed
330 needle-shaped CaSO₄ crystals in the Ca(NO₃)₂ droplet via the multiphase reaction of SO₂ with NO₂. The sulfate
331 formation was observed only during the multiphase oxidation by NO₂, that is, after the complete conversion of
332 CaCO₃ to Ca(NO₃)₂ droplet. The precipitation of CaSO₄ from solution promoted sulfate formation. The reactive
333 uptake coefficient of SO₂ for sulfate formation in the multiphase reaction with NO₂ is on the order of 10⁻⁸ under
334 the experimental conditions of this study (RH: 46-72%, NO₂: 75 ppm). The reactive uptake coefficient of SO₂
335 was found to be enhanced at higher RH.

336 In order to assess the importance of the multiphase reaction of SO₂ directly oxidized by NO₂ to sulfate in the
337 atmosphere, we compare the lifetime of SO₂ due to the multiphase oxidation of SO₂ by NO₂ with the lifetime due
338 to the gas phase oxidation of SO₂ by OH. Using a daytime OH concentration of 1×10⁶ molecule cm⁻³ (Lelieveld
339 et al., 2016; Prinn et al., 2005), the lifetime of SO₂ in the atmosphere due to gas phase OH oxidation is around 12
340 days. The life time of SO₂ due to the multiphase oxidation by NO₂ is around 7000 days using the uptake
341 coefficient of SO₂ from this study (3.22×10⁻⁸) and a typical particle surface area concentration for mineral
342 aerosols in winter in Beijing (6.3×10⁻⁶ cm² cm⁻³) (Huang et al., 2015). Using an annual average particle surface
343 area concentration of PM₁₀ in Beijing (1.4×10⁻⁵ cm² cm⁻³)(Wehner et al., 2008) results in a SO₂ life time of 3300
344 days due to the multiphase oxidation by NO₂. In the atmosphere, the lifetime of SO₂ due to the multiphase
345 oxidation by NO₂ should be even longer than these values because the uptake coefficient of SO₂ used here
346 (3.22×10⁻⁸) is an upper limit of the uptake coefficient of SO₂ in the ambient atmosphere as discussed above. This
347 comparison indicates that the direct multiphase oxidation of SO₂ by NO₂ is unlikely to be an important sink of
348 SO₂ and source of sulfate compared with the oxidation of SO₂ by OH.

349 In this study, we investigated the multiphase oxidation of SO₂ directly by NO₂ via using inert N₂ as a carrier
350 gas and assessed the importance of this reaction in the atmosphere. Although the oxidation of SO₂ by NO₂ alone

351 unlikely contributes significantly to sulfate formation, NO_2 may facilitate the oxidation of SO_2 by other oxidants.
352 For example, in the ambient atmosphere, O_2 is abundantly present and previous studies have suggested that O_2
353 can oxidize sulfite in the presence of NO_2 in bulk aqueous solution (Littlejohn et al., 1993). Therefore, the
354 potential synergy of NO_2 and other multiphase oxidation pathways of SO_2 on aqueous aerosol particles warrants
355 further studies. We will address the synergy of NO_2 and the multiphase oxidation of SO_2 by O_2 in a companion
356 paper.

357 Despite the less important role in sulfate formation, the multiphase oxidation of SO_2 by NO_2 on CaCO_3
358 particles helps interpreting the findings from field studies. For example, internally mixed CaCO_3 with $\text{Ca}(\text{NO}_3)_2$
359 and CaSO_4 particles with varying reacted fractions of CaCO_3 were observed in the field (Hwang and Ro, 2006; Li
360 and Shao, 2009), but how the internally mixed particles are formed is not clear. In this study we showed that
361 CaSO_4 can be formed inside the $\text{Ca}(\text{NO}_3)_2$ droplet after the deliquescence of initially produced $\text{Ca}(\text{NO}_3)_2$ through
362 the reaction of SO_2 with NO_2 . In this way, internally mixed CaCO_3 with $\text{Ca}(\text{NO}_3)_2$ and CaSO_4 particles can be
363 formed. Moreover, Hwang and Ro (2006) found that CaSO_4 -containing particles were observed to be almost
364 always internally mixed with nitrate. The multiphase reaction process of SO_2 with NO_2 on CaCO_3 particles found
365 this study can also explain this finding.

366

367 **Acknowledgements**

368 This work was supported by Natural Science Foundation Committee of China (41421064, 21190051,
369 40490265) and Ministry of Science and Technology (Grant No. 2002CB410802).

370 **References**

- 371 Al-Abadleh, H. A., Krueger, B. J., Ross, J. L., and Grassian, V. H.: Phase transitions in calcium nitrate thin films, *Chem.*
372 *Commun.*, 2796-2797, 2003.
- 373 Cao, J. J., Lee, S. C., Zhang, X. Y., Chow, J. C., An, Z. S., Ho, K. F., Watson, J. G., Fung, K., Wang, Y. Q., and Shen, Z. X.:
374 Characterization of airborne carbonate over a site near Asian dust source regions during spring 2002 and its climatic and
375 environmental significance, *J. Geophys. Res.-Atmos.*, 110, 10.1029/2004jd005244, 2005.
- 376 Cheng, Y., Zheng, G., Wei, C., Mu, Q., Zheng, B., Wang, Z., Gao, M., Zhang, Q., He, K., Carmichael, G., Pöschl, U., and
377 Su, H.: Reactive nitrogen chemistry in aerosol water as a source of sulfate during haze events in China, *Sci. Adv.*, 2, 2016a.
- 378 Cheng, Y. F., Zheng, G. J., Wei, C., Mu, Q., Zheng, B., Wang, Z. B., Gao, M., Zhang, Q., He, K. B., Carmichael, G., Poschl,
379 U., and Su, H.: Reactive nitrogen chemistry in aerosol water as a source of sulfate during haze events in China, *Sci. Adv.*, 2,
380 10.1126/sciadv.1601530, 2016b.
- 381 Chu, B. W., Zhang, X., Liu, Y. C., He, H., Sun, Y., Jiang, J. K., Li, J. H., and Hao, J. M.: Synergetic formation of secondary
382 inorganic and organic aerosol: effect of SO₂ and NH₃ on particle formation and growth, *Atmos. Chem. Phys.*, 16,
383 14219-14230, 10.5194/acp-16-14219-2016, 2016.
- 384 Clifton, C. L., Altstein, N., and Huie, R. E.: Rate-constant for the reaction of NO₂ with sulfur(IV) over the pH range 5.3-13,
385 *Environ. Sci. Technol.*, 22, 586-589, 10.1021/es00170a018, 1988.
- 386 Cui, H. X., Cheng, T. T., Chen, J. M., Xu, Y. F., and Fang, W.: A Simulated Heterogeneous Reaction of SO₂ on the Surface
387 of Hematite at Different Temperatures, *Acta Phys. Chim. Sin.*, 24, 2331-2336, 10.3866/pku.whxb20081231, 2008.
- 388 Davidovits, P., Kolb, C. E., Williams, L. R., Jayne, J. T., and Worsnop, D. R.: Mass accommodation and chemical reactions
389 at gas-liquid interfaces, *Chem. Rev.*, 106, 1323-1354, 10.1021/cr040366k, 2006.
- 390 Ellison, T. K., and Eckert, C. A.: The oxidation of aqueous sulfur dioxide. 4. The influence of nitrogen dioxide at low pH, *J.*
391 *Phys. Chem.*, 88, 2335-2339, 10.1021/j150655a030, 1984.
- 392 Finlayson-Pitts, B., and Pitts Jr., J.: *Chemistry of the upper and lower atmosphere: theory, experiments, and applications*,
393 Academic Press San Diego, 969 pp., 1999.
- 394 Fu, X., Wang, S. X., Chang, X., Cai, S. Y., Xing, J., and Hao, J. M.: Modeling analysis of secondary inorganic aerosols over
395 China: pollution characteristics, and meteorological and dust impacts, *Sci. Rep.*, 6, 10.1038/srep35992, 2016.
- 396 Gao, M., Carmichael, G. R., Wang, Y., Ji, D., Liu, Z., and Wang, Z.: Improving simulations of sulfate aerosols during winter
397 haze over Northern China: the impacts of heterogeneous oxidation by NO₂, *Front. Environ. Sci. Eng.*, 10, 16,
398 10.1007/s11783-016-0878-2, 2016.
- 399 Good, R. J., and Koo, M. N.: Effect of drop size on contact-angle, *J. Colloid Interface Sci.*, 71, 283-292, 1979.
- 400 Goodman, A. L., Li, P., Usher, C. R., and Grassian, V. H.: Heterogeneous uptake of sulfur dioxide on aluminum and
401 magnesium oxide particles, *J. Phys. Chem. A* 105, 6109-6120, 2001.
- 402 Guo, S., Hu, M., Zamora, M. L., Peng, J., Shang, D., Zheng, J., Du, Z., Wu, Z., Shao, M., Zeng, L., Molina, M. J., and Zhang,
403 R.: Elucidating severe urban haze formation in China, *Proc. Nat. Acad. Sci. U.S.A.*, 111, 17373-17378,
404 10.1073/pnas.1419604111, 2014.
- 405 He, H., Wang, Y., Ma, Q., Ma, J., Chu, B., Ji, D., Tang, G., Liu, C., Zhang, H., and Hao, J.: Mineral dust and NO_x promote
406 the conversion of SO₂ to sulfate in heavy pollution days, *Sci. Rep.*, 4, 10.1038/srep04172, 2014.
- 407 Huang, L., Zhao, Y., Li, H., and Chen, Z.: Kinetics of Heterogeneous Reaction of Sulfur Dioxide on Authentic Mineral Dust:
408 Effects of Relative Humidity and Hydrogen Peroxide, *Environ. Sci. Technol.*, 49, 10797-10805, 10.1021/acs.est.5b03930,
409 2015.
- 410 Huang, L. B., Zhao, Y., Li, H., and Chen, Z. M.: Hydrogen peroxide maintains the heterogeneous reaction of sulfur dioxide
411 on mineral dust proxy particles, *Atmos. Environ.*, 141, 552-559, 10.1016/j.atmosenv.2016.07.035, 2016.

412 Huang, X., Song, Y., Zhao, C., Li, M., Zhu, T., Zhang, Q., and Zhang, X.: Pathways of sulfate enhancement by natural and
413 anthropogenic mineral aerosols in China, *J. Geophys. Res.-Atmos.*, 119, 14,165-114,179, 10.1002/2014jd022301, 2014.

414 Hwang, H. J., and Ro, C. U.: Direct observation of nitrate and sulfate formations from mineral dust and sea-salts using low-Z
415 particle electron probe X-ray microanalysis, *Atmos. Environ.*, 40, 3869-3880, 10.1016/j.atmosenv.2006.02.022, 2006.

416 Kong, L. D., Zhao, X., Sun, Z. Y., Yang, Y. W., Fu, H. B., Zhang, S. C., Cheng, T. T., Yang, X., Wang, L., and Chen, J. M.:
417 The effects of nitrate on the heterogeneous uptake of sulfur dioxide on hematite, *Atmos. Chem. Phys.*, 14, 9451-9467,
418 10.5194/acp-14-9451-2014, 2014.

419 Krueger, B. J., Grassian, V. H., Cowin, J. P., and Laskin, A.: Heterogeneous chemistry of individual mineral dust particles
420 from different dust source regions: the importance of particle mineralogy, *Atmos. Environ.*, 38, 6253-6261,
421 10.1016/j.atmosenv.2004.07.010, 2004.

422 Lee, Y.-N., and Schwartz, S. E.: Kinetics of oxidation of aqueous sulfur (IV) by nitrogen dioxide, in: *Precipitation*
423 *Scavenging, Dry Deposition and Resuspension*, edited by: Pruppacher, H. R., Semonin, R. G., and Slinn, W. G. N., Elsevier,
424 New York, 453-466, 1983.

425 Lelieveld, J., Gromov, S., Pozzer, A., and Taraborrelli, D.: Global tropospheric hydroxyl distribution, budget and reactivity,
426 *Atmos. Chem. Phys.*, 16, 12477-12493, 10.5194/acp-16-12477-2016, 2016.

427 Li, H. J., Zhu, T., Zhao, D. F., Zhang, Z. F., and Chen, Z. M.: Kinetics and mechanisms of heterogeneous reaction of NO₂
428 on CaCO₃ surfaces under dry and wet conditions, *Atmos. Chem. Phys.*, 10, 463-474, 2010.

429 Li, J., Shang, J., and Zhu, T.: Heterogeneous reactions of SO₂ on ZnO particle surfaces, *Sci. China Chem.*, 54, 161-166,
430 10.1007/s11426-010-4167-9, 2011.

431 Li, L., Chen, Z. M., Ding, J., Zhu, T., and Zhang, Y. H.: A DRIFTS study of SO₂ oxidation on the surface of CaCO₃
432 particles, *Spectrosc. Spect. Anal.*, 24, 1556-1559, 2004.

433 Li, L., Chen, Z. M., Zhang, Y. H., Zhu, T., Li, J. L., and Ding, J.: Kinetics and mechanism of heterogeneous oxidation of
434 sulfur dioxide by ozone on surface of calcium carbonate, *Atmos. Chem. Phys.*, 6, 2453-2464, 2006.

435 Li, L., Chen, Z. M., Zhang, Y. H., Zhu, T., Li, S., Li, H. J., Zhu, L. H., and Xu, B. Y.: Heterogeneous oxidation of sulfur
436 dioxide by ozone on the surface of sodium chloride and its mixtures with other components, *J. Geophys. Res.-Atmos.*, 112,
437 10.1029/2006jd008207, 2007.

438 Li, W. J., and Shao, L. Y.: Observation of nitrate coatings on atmospheric mineral dust particles, *Atmos. Chem. Phys.*, 9,
439 1863-1871, 2009.

440 Lide, D. R.: *CRC Handbook of Chemistry and Physics*, 89 ed., CRC Press/Taylor and Francis, Boca Raton, FL, 2009.

441 Littlejohn, D., Wang, Y. Z., and Chang, S. G.: Oxidation of aqueous sulfite ion by nitrogen-dioxide, *Environ. Sci. Technol.*,
442 27, 2162-2167, 10.1021/es00047a024, 1993.

443 Liu, C., Ma, Q. X., Liu, Y. C., Ma, J. Z., and He, H.: Synergistic reaction between SO₂ and NO₂ on mineral oxides: a
444 potential formation pathway of sulfate aerosol, *Phys. Chem. Chem. Phys.*, 14, 1668-1676, 10.1039/c1cp22217a, 2012.

445 Liu, Y. J., Zhu, T., Zhao, D. F., and Zhang, Z. F.: Investigation of the hygroscopic properties of Ca(NO₃)₂ and internally
446 mixed Ca(NO₃)₂/CaCO₃ particles by micro-Raman spectrometry, *Atmos. Chem. Phys.*, 8, 7205-7215, 2008.

447 Ma, Q., He, H., Liu, Y., Liu, C., and Grassian, V. H.: Heterogeneous and multiphase formation pathways of gypsum in the
448 atmosphere, *Phys. Chem. Chem. Phys.*, 15, 19196-19204, 10.1039/c3cp53424c, 2013a.

449 Ma, Q., Wang, T., Liu, C., He, H., Wang, Z., Wang, W., and Liang, Y.: SO₂ Initiates the Efficient Conversion of NO₂ to
450 HONO on MgO Surface, *Environ. Sci. Technol.*, 51, 3767-3775, 10.1021/acs.est.6b05724, 2017.

451 Ma, Q. X., Liu, Y. C., and He, H.: Synergistic effect between NO₂ and SO₂ in their adsorption and reaction on
452 gamma-alumina, *J. Phys. Chem. A* 112, 6630-6635, 10.1021/jp802025z, 2008.

453 Ma, Q. X., He, H., Liu, Y. C., Liu, C., and Grassian, V. H.: Heterogeneous and multiphase formation pathways of gypsum in
454 the atmosphere, *Phys. Chem. Chem. Phys.*, 15, 19196-19204, 10.1039/c3cp53424c, 2013b.

455 Martin, L. R., Damschen, D. E., and Judeikis, H. S.: The reactions of nitrogen-oxides with SO₂ in aqueous aerosols, *Atmos.*
456 *Environ.*, 15, 191-195, 10.1016/0004-6981(81)90010-x, 1981.

457 Nakamoto, K.: *Infrared and Raman Spectra of Inorganic and Coordination Compounds*, John Wiley & Sons, New York,
458 1997.

459 Nash, T.: Effect of nitrogen-dioxide and of some transition-metals on the oxidation of dilute bisulfite solutions, *Atmos.*
460 *Environ.*, 13, 1149-1154, 10.1016/0004-6981(79)90038-6, 1979.

461 Okada, K., Qin, Y., and Kai, K.: Elemental composition and mixing properties of atmospheric mineral particles collected in
462 Hohhot, China, *Atmos. Res.*, 73, 45-67, 2005.

463 Park, J. Y., and Jang, M.: Heterogeneous photooxidation of sulfur dioxide in the presence of airborne mineral dust particles,
464 *Rsc Advances*, 6, 58617-58627, 10.1039/c6ra09601h, 2016.

465 Passananti, M., Kong, L. D., Shang, J., Dupart, Y., Perrier, S., Chen, J. M., Donaldson, D. J., and George, C.: Organosulfate
466 Formation through the Heterogeneous Reaction of Sulfur Dioxide with Unsaturated Fatty Acids and Long-Chain Alkenes,
467 *Angew. Chem.-Int. Edit.*, 55, 10336-10339, 10.1002/anie.201605266, 2016.

468 Prince, A. P., Grassian, V. H., Kleiber, P., and Young, M. A.: Heterogeneous conversion of calcite aerosol by nitric acid,
469 *Phys. Chem. Chem. Phys.*, 9, 622-634, 2007a.

470 Prince, A. P., Kleiber, P., Grassian, V. H., and Young, M. A.: Heterogeneous interactions of calcite aerosol with sulfur
471 dioxide and sulfur dioxide-nitric acid mixtures, *Phys. Chem. Chem. Phys.*, 9, 3432-3439, 2007b.

472 Prinn, R. G., Huang, J., Weiss, R. F., Cunnold, D. M., Fraser, P. J., Simmonds, P. G., McCulloch, A., Harth, C., Reimann, S.,
473 Salameh, P., O'Doherty, S., Wang, R. H. J., Porter, L. W., Miller, B. R., and Krummel, P. B.: Evidence for variability of
474 atmospheric hydroxyl radicals over the past quarter century, *Geophys. Res. Lett.*, 32, 10.1029/2004gl022228, 2005.

475 Rosenberg, H. S., and Grotta, H. M.: Nitrogen oxides (NO_x) influence on sulfite oxidation and scaling in lime/limestone flue
476 gas desulfurization (FGD) systems, *Environ. Sci. Technol.*, 14, 470-472, 10.1021/es60164a011, 1980.

477 Sarma, L. P., Prasad, P. S. R., and Ravikumar, N.: Raman spectroscopic study of phase transitions in natural gypsum, *J.*
478 *Raman Spectrosc.*, 29, 851-856, 10.1002/(sici)1097-4555(199809)29:9<851::aid-jrs313>3.0.co;2-s, 1998.

479 Seinfeld, J. H., and Pandis, S. N.: *Atmospheric chemistry and physics: from air pollution to climate change*, 2nd ed., John
480 Wiley & Sons. Inc., 2006.

481 Shang, J., Li, J., and Zhu, T.: Heterogeneous reaction of SO₂ on TiO₂ particles, *Sci. China Chem.*, 53, 2637-2643,
482 10.1007/s11426-010-4160-3, 2010.

483 Shen, C. H., and Rochelle, G. T.: Nitrogen Dioxide Absorption and Sulfite Oxidation in Aqueous Sulfite, *Environ. Sci.*
484 *Technol.*, 32, 1994-2003, 10.1021/es970466q, 1998.

485 Song, C. H., Maxwell-Meier, K., Weber, R. J., Kapustin, V., and Clarke, A.: Dust composition and mixing state inferred
486 from airborne composition measurements during ACE-Asia C130 Flight #6, *Atmos. Environ.*, 39, 359-369, 2005.

487 Sorimachi, A., Sakai, M., Ishitani, O., Nishikawa, M., and Sakamoto, K.: Study on dry deposition of SO₂-NO_x onto loess,
488 *Water Air Soil Pollut.*, 130, 541-546, 10.1023/a:1013834729728, 2001.

489 Takeuchi, H., Ando, M., and Kizawa, N.: Absorption of Nitrogen Oxides in Aqueous Sodium Sulfite and Bisulfite Solutions,
490 *Industrial & Engineering Chemistry Process Design and Development*, 16, 303-308, 10.1021/i260063a010, 1977.

491 Tan, F., Jing, B., Tong, S. R., and Ge, M. F.: The effects of coexisting Na₂SO₄ on heterogeneous uptake of NO₂ on CaCO₃
492 particles at various RHs, *Sci. Total Environ.*, 586, 930-938, 10.1016/j.scitotenv.2017.02.072, 2017.

493 Tang, I. N., and Fung, K. H.: Hydration and Raman scattering studies of levitated microparticles: Ba(NO₃)(2), Sr(NO₃)(2),
494 and Ca(NO₃)(2), *J. Chem. Phys.*, 106, 1653-1660, 1997.

495 Tursic, J., and Grgic, I.: Influence of NO₂ on S(IV) oxidation in aqueous suspensions of aerosol particles from two different
496 origins, *Atmos. Environ.*, 35, 3897-3904, 10.1016/s1352-2310(01)00142-x, 2001.

497 Ullerstam, M., Vogt, R., Langer, S., and Ljungstrom, E.: The kinetics and mechanism of SO₂ oxidation by O₃ on mineral
498 dust, *Phys. Chem. Chem. Phys.*, 4, 4694-4699, 10.1039/b203529b, 2002.

499 Ullerstam, M., Johnson, M. S., Vogt, R., and Ljungstrom, E.: DRIFTS and Knudsen cell study of the heterogeneous
500 reactivity of SO₂ and NO₂ on mineral dust, *Atmos. Chem. Phys.*, 3, 2043-2051, 2003.

501 Wang, G., Zhang, R., Gomez, M. E., Yang, L., Levy Zamora, M., Hu, M., Lin, Y., Peng, J., Guo, S., Meng, J., Li, J., Cheng,
502 C., Hu, T., Ren, Y., Wang, Y., Gao, J., Cao, J., An, Z., Zhou, W., Li, G., Wang, J., Tian, P., Marrero-Ortiz, W., Secret, J.,
503 Du, Z., Zheng, J., Shang, D., Zeng, L., Shao, M., Wang, W., Huang, Y., Wang, Y., Zhu, Y., Li, Y., Hu, J., Pan, B., Cai, L.,
504 Cheng, Y., Ji, Y., Zhang, F., Rosenfeld, D., Liss, P. S., Duce, R. A., Kolb, C. E., and Molina, M. J.: Persistent sulfate
505 formation from London Fog to Chinese haze, *Proc. Nat. Acad. Sci. U.S.A.*, 113, 13630-13635, 10.1073/pnas.1616540113,
506 2016.

507 Wang, Y. S., Yao, L., Wang, L. L., Liu, Z. R., Ji, D. S., Tang, G. Q., Zhang, J. K., Sun, Y., Hu, B., and Xin, J. Y.:
508 Mechanism for the formation of the January 2013 heavy haze pollution episode over central and eastern China, *Sci. China
509 Earth Sci.*, 57, 14-25, 10.1007/s11430-013-4773-4, 2014a.

510 Wang, Y. X., Zhang, Q. Q., Jiang, J. K., Zhou, W., Wang, B. Y., He, K. B., Duan, F. K., Zhang, Q., Philip, S., and Xie, Y.
511 Y.: Enhanced sulfate formation during China's severe winter haze episode in January 2013 missing from current models, *J.
512 Geophys. Res.-Atmos.*, 119, 10.1002/2013jd021426, 2014b.

513 Wehner, B., Birmili, W., Ditas, F., Wu, Z., Hu, M., Liu, X., Mao, J., Sugimoto, N., and Wiedensohler, A.: Relationships
514 between submicrometer particulate air pollution and air mass history in Beijing, China, 2004–2006, *Atmos. Chem. Phys.*, 8,
515 6155-6168, 10.5194/acp-8-6155-2008, 2008.

516 Wu, L. Y., Tong, S. R., Wang, W. G., and Ge, M. F.: Effects of temperature on the heterogeneous oxidation of sulfur dioxide
517 by ozone on calcium carbonate, *Atmos. Chem. Phys.*, 11, 6593-6605, 10.5194/acp-11-6593-2011, 2011.

518 Wu, L. Y., Tong, S. R., Zhou, L., Wang, W. G., and Ge, M. F.: Synergistic Effects between SO₂ and HCOOH on
519 alpha-Fe₂O₃, *J. Phys. Chem. A* 117, 3972-3979, 10.1021/jp400195f, 2013.

520 Wu, L. Y., Tong, S. R., and Ge, M. F.: Synergistic Effect between SO₂ and HCOOH on the Surface of CaO, *Acta Chim.
521 Sinica* 73, 131-136, 10.6023/a14120875, 2015.

522 Xie, Y. N., Ding, A. J., Nie, W., Mao, H. T., Qi, X. M., Huang, X., Xu, Z., Kerminen, V. M., Petaja, T., Chi, X. G., Virkkula,
523 A., Boy, M., Xue, L. K., Guo, J., Sun, J. N., Yang, X. Q., Kulmala, M., and Fu, C. B.: Enhanced sulfate formation by
524 nitrogen dioxide: Implications from in situ observations at the SORPES station, *J. Geophys. Res.-Atmos.*, 120, 12679-12694,
525 10.1002/2015jd023607, 2015.

526 Xue, J., Yuan, Z. B., Griffith, S. M., Yu, X., Lau, A. K. H., and Yu, J. Z.: Sulfate Formation Enhanced by a Cocktail of High
527 NO_x, SO₂, Particulate Matter, and Droplet pH during Haze-Fog Events in Megacities in China: An Observation-Based
528 Modeling Investigation, *Environ. Sci. Technol.*, 50, 7325-7334, 10.1021/acs.est.6b00768, 2016.

529 Zhang, D. Z., Shi, G. Y., Iwasaka, Y., and Hu, M.: Mixture of sulfate and nitrate in coastal atmospheric aerosols: individual
530 particle studies in Qingdao (36 degrees 04 ' N, 120 degrees 21 ' E), China, *Atmos. Environ.*, 34, 2669-2679,
531 10.1016/s1352-2310(00)00078-9, 2000.

532 Zhang, J. K., Sun, Y., Liu, Z. R., Ji, D. S., Hu, B., Liu, Q., and Wang, Y. S.: Characterization of submicron aerosols during a
533 month of serious pollution in Beijing, 2013, *Atmos. Chem. Phys.*, 14, 2887-2903, 10.5194/acp-14-2887-2014, 2014.

534 Zhang, Q., Jimenez, J. L., Canagaratna, M. R., Allan, J. D., Coe, H., Ulbrich, I., Alfarra, M. R., Takami, A., Middlebrook, A.
535 M., Sun, Y. L., Dzepina, K., Dunlea, E., Docherty, K., DeCarlo, P. F., Salcedo, D., Onasch, T., Jayne, J. T., Miyoshi, T.,
536 Shimono, A., Hatakeyama, S., Takegawa, N., Kondo, Y., Schneider, J., Drewnick, F., Borrmann, S., Weimer, S., Demerjian,
537 K., Williams, P., Bower, K., Bahreini, R., Cottrell, L., Griffin, R. J., Rautiainen, J., Sun, J. Y., Zhang, Y. M., and Worsnop,
538 D. R.: Ubiquity and dominance of oxygenated species in organic aerosols in anthropogenically-influenced Northern
539 Hemisphere midlatitudes, *Geophys. Res. Lett.*, 34, 10.1029/2007gl029979, 2007.

540 Zhao, D., Zhu, T., and Song, X.: Phase change of particles by heterogeneous reactions enhances aerosol production rate in
541 the atmosphere, in preparation, 2017.

542 Zhao, D. F., Zhu, T., Chen, Q., Liu, Y. J., and Zhang, Z. F.: Raman micro-spectrometry as a technique for investigating
543 heterogeneous reactions on individual atmospheric particles, *Sci. China Chem.*, 54, 154-160, 10.1007/s11426-010-4182-x,
544 2011.

545 Zhao, X., Kong, L. D., Sun, Z. Y., Ding, X. X., Cheng, T. T., Yang, X., and Chen, J. M.: Interactions between
546 Heterogeneous Uptake and Adsorption of Sulfur Dioxide and Acetaldehyde on Hematite, *J. Phys. Chem. A* 119, 4001-4008,
547 10.1021/acs.jpca.5b01359, 2015.

548 Zheng, B., Zhang, Q., Zhang, Y., He, K. B., Wang, K., Zheng, G. J., Duan, F. K., Ma, Y. L., and Kimoto, T.: Heterogeneous
549 chemistry: a mechanism missing in current models to explain secondary inorganic aerosol formation during the January 2013
550 haze episode in North China, *Atmos. Chem. Phys.*, 15, 2031-2049, 10.5194/acp-15-2031-2015, 2015a.

551 Zheng, G. J., Duan, F. K., Su, H., Ma, Y. L., Cheng, Y., Zheng, B., Zhang, Q., Huang, T., Kimoto, T., Chang, D., Poschl, U.,
552 Cheng, Y. F., and He, K. B.: Exploring the severe winter haze in Beijing: the impact of synoptic weather, regional transport
553 and heterogeneous reactions, *Atmos. Chem. Phys.*, 15, 2969-2983, 10.5194/acp-15-2969-2015, 2015b.

554 Zhou, L., Wang, W. G., Gai, Y. B., and Ge, M. F.: Knudsen cell and smog chamber study of the heterogeneous uptake of
555 sulfur dioxide on Chinese mineral dust, *J. Environ. Sci.*, 26, 2423-2433, 10.1016/j.jes.2014.04.005, 2014.

556 Zhu, T., Shang, J., and Zhao, D. F.: The roles of heterogeneous chemical processes in the formation of an air pollution
557 complex and gray haze, *Sci. China Chem.*, 54, 145-153, 10.1007/s11426-010-4181-y, 2011.

558

560

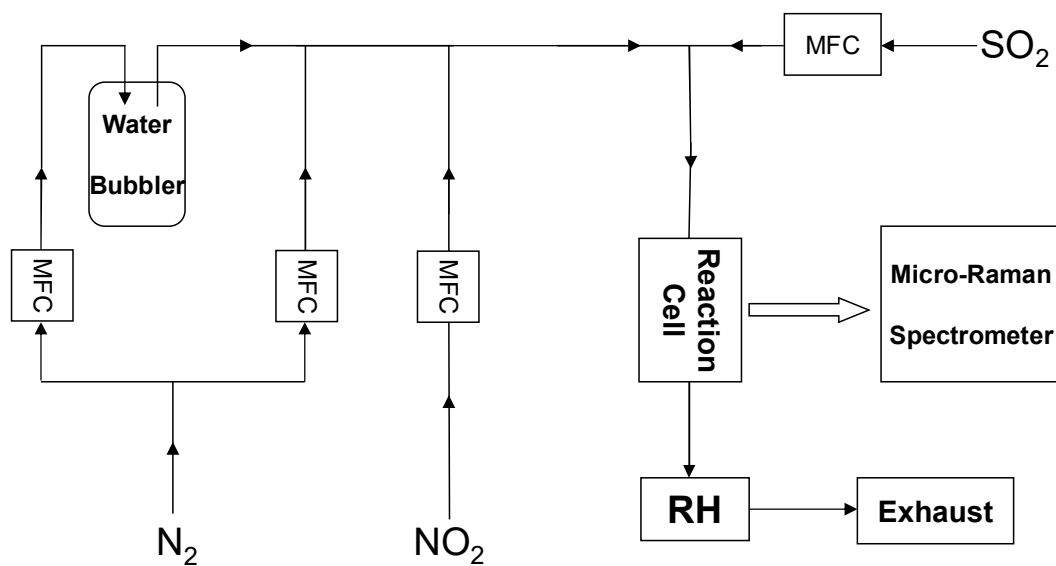
Table 1 Summary of the results obtained in different reaction systems

Particle	Gases	RH (%)	Whether sulfate was detected
CaCO ₃	SO ₂ (75 ppm)+NO ₂ (75 ppm)	72	Yes
Ca(NO ₃) ₂ droplet	SO ₂ (75 ppm)+NO ₂ (75 ppm)	72	Yes
CaCO ₃	SO ₂ (150 ppm)	72	No
Ca(NO ₃) ₂ droplet	SO ₂ (150 ppm))	72	No
NaNO ₃ droplet	SO ₂ (75 ppm)+NO ₂ (75 ppm)	72	No
NH ₄ NO ₃ droplet	SO ₂ (75 ppm)+NO ₂ (75 ppm)	72	No

563 Table 2. Reactive uptake coefficient of SO₂ for sulfate formation (γ) during the reaction of SO₂ with NO₂ on
564 individual CaCO₃ particles under different conditions at 298 K.

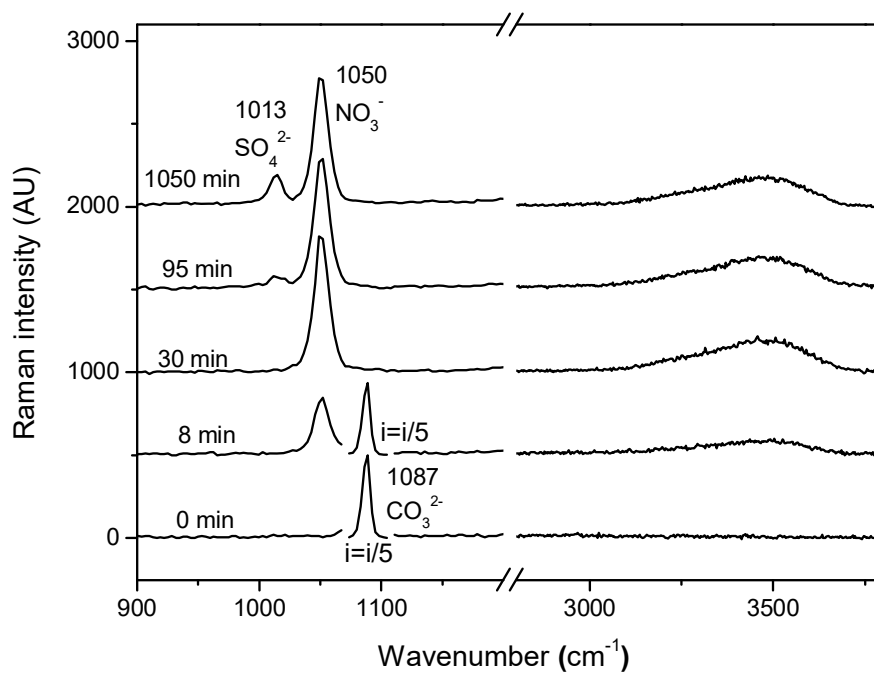
[SO ₂] (ppm)	[NO ₂] (ppm)	RH (%)	γ ($\times 10^{-8}$)
75	75	72	3.22 \pm 1.08
75	200	72	16.0 \pm 3.12
75	75	46	3.22 \pm 0.90
75	75	17	0 ^a
200	200	17	0 ^a

565 ^a: Sulfate was below the detection limit.



566

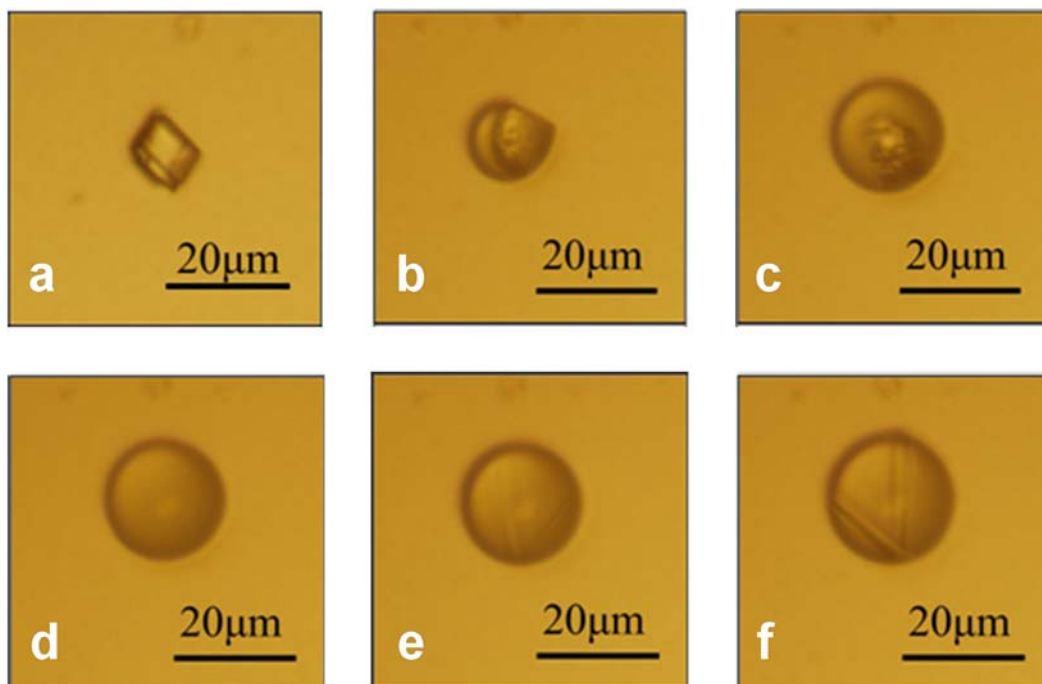
567 Fig. 1. Schematic diagram of the experimental setup. MFC: mass flow controller.



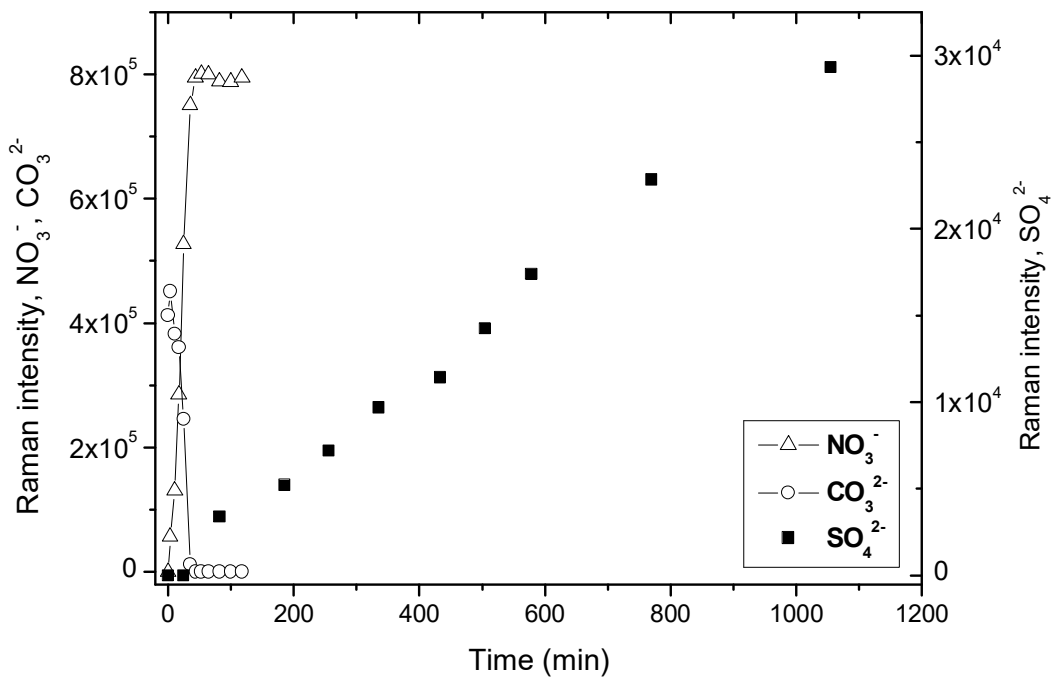
568

569 Fig. 2. Raman spectra of an individual CaCO₃ particle during the reaction with NO₂ (75 ppm) and SO₂ (75 ppm)

570 at 72% RH at the reaction time of 0, 8, 30, 95, and 1050 min.



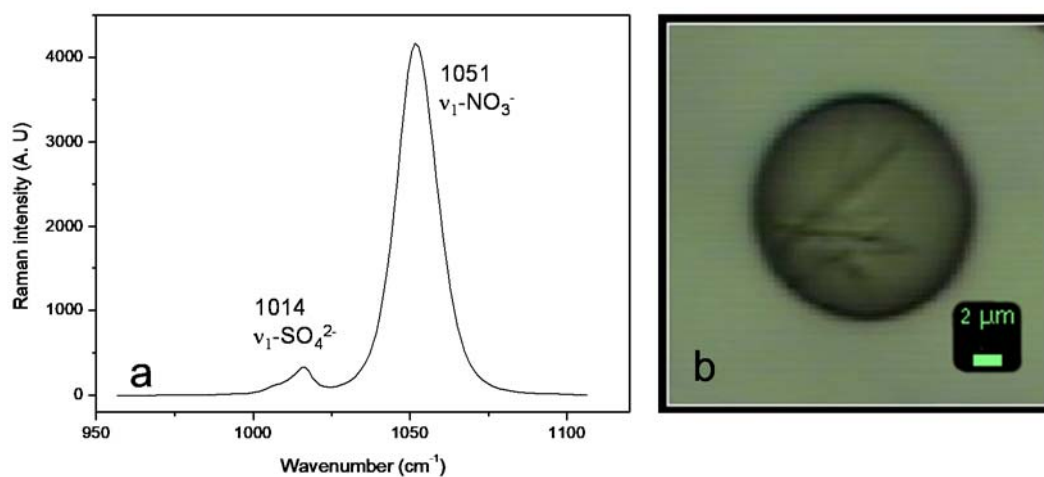
571
572 Fig. 3. Microscopic images of an individual CaCO_3 particle (same as in Fig. 2) reacting with NO_2 (75 ppm) and
573 SO_2 (75 ppm) at 72% RH. a-f corresponds to the reaction time of 0, 6, 29, 37, 94, and 1050 min, respectively.
574



575

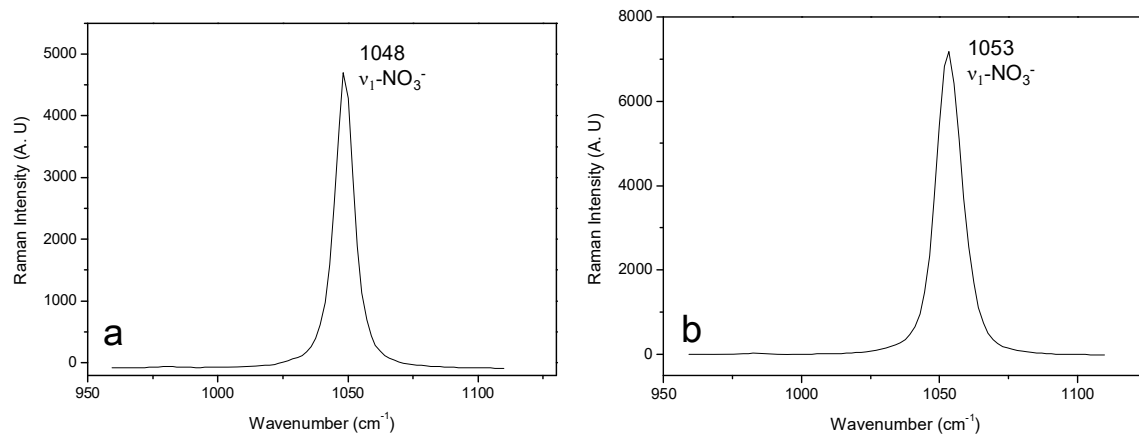
576 Fig. 4. Raman peak intensity of carbonate, nitrate (left axis), and sulfate (right axis) as a function of time during
 577 the reaction of an individual CaCO₃ particle with NO₂ (75ppm) and SO₂ (75ppm) at 72% RH (same as in Fig. 2
 578 and 3). Note that the scales of the left axis and right axis are different. The intensity of NO₃⁻, SO₄²⁻, and CO₃²⁻
 579 show the peak area at 1050, 1013, and 1087 cm⁻¹, respectively, in Raman spectra obtained by Raman mapping.
 580 By 118 min, CaCO₃ was completely converted to Ca(NO₃)₂. Carbonate had decreased to zero and nitrate had
 581 reached a plateau. Therefore no further data of carbonate and nitrate were shown.

582



584

585 Fig. 5. Raman spectra (a) and microscopic image (b) of a $\text{Ca}(\text{NO}_3)_2$ droplet reacting with NO_2 (75 ppm) and SO_2
586 (75 ppm) at 72% RH at a reaction time of 300 min. The peak at 1014 cm^{-1} in Raman spectra and crystals from the
587 microscopic image indicate CaSO_4 was formed in this reaction.



589

590 Fig. 6. Raman spectra of a NH_4NO_3 (a) and NaNO_3 (b) droplet reacting with NO_2 (75 ppm) and SO_2 (75 ppm) at
591 72% RH at the reaction time of 300 min.

592